Journal of Microwaves, Optoelectronics and Electromagnetic Applications, Vol. 21, No. 1, March 2022
DOI: http://dx.doi.org/10.1590/2179-10742022v21i11306

Bandpass Filter Using SIW Technology in Inductive Window Topology with Low-Cost Substrate FR-4

Marcio L. Michalkiewicz[1], Andre A. Mariano[1], Cesar A. Dartora[1], Fernando C. Castaldo[2]
[1]*Federal University of Parana, Curitiba, Parana, Brazil – marciomichal@gmail.com, mariano@ufpr.br, cadartora@eletrica.ufpr.br*
[2]*Federal University of Technology Parana, Curitiba, Parana, Brazil – castaldofc@hotmail.com*

***Abstract*—This paper features a step-by-step procedure for designing, simulate, and manufacture a bandpass filter using an inductive window topology within the substrate integrated waveguide (SIW) technology. We have chosen an operating frequency in the microwave range compatible with IoT circuits, employing a dielectric material, the FR-4, which is low cost and widely accessible. Even though it is not the most suitable material for microwave circuits operating above a few gigahertz, we propose to evaluate the challenges it poses on the filter design, in addition to performing a comparison between the results obtained directly from the analytical method, the computational simulations and measured results in the built prototype.**

***Index Terms*—** Bandpass filter, SIW, microstrip, FR-4

I. INTRODUCTION

Newly developed technologies demand constant advancements in engineering techniques. Thus, high-frequency circuits have undergone an extraordinary evolution in recent decades. Such reality has been enhanced mainly by the increase in data traffic and the consequent depletion of available bandwidth. Electromagnetic bandwidth, however, is a scarce resource, as it follows strict rules for its use, and it is the lack of free channel in the radio frequency and microwave bands that pressures industries to develop new systems with ever higher frequencies [1].

All this context certainly motivated the research of Hirokawa [2] and Uchimura [3], who were the first to describe circuits using a new technology, which became known as *Substrate Integrated Waveguide* (SIW). The SIW technology combines the advantages of planar technology and classic metallic waveguides in a complementary way. Its components are light and compact. They use a cheap and well-established manufacturing process: the printed circuits boards (using materials like ceramic, Teflon™ and others). At the same time, they also exhibit a high-power capacity and electromagnetic shielding, native to the technology, practically perfect. However, the most significant advantage of SIW is that it integrates a complete system on a single substrate, including passive components, active components, chipsets, and antennas. Today, a "state-of-the-art" in that matter presents circuits operating at frequencies in the order of terahertz, silicon-based substrate integrated waveguides and air-dielectric-integrated substrate waveguides, which have shown to be very

Brazilian Microwave and Optoelectronics Society-SBMO *received 15 Apr 2021; for review 15 May 2021; accepted 2 Dec 2021*
Brazilian Society of Electromagnetism-SBMag *ISSN 2179-1074*

promising, among many applications as mobile communications, radars for autonomous automobiles and especially for IoT (Internet of Things).

As we can see, SIW technology is involved in some of the most important vectors of the 4.0 industry. A survey of the top executives of large technology companies revealed that 72% of respondents believe that of the emerging technologies, IoT will have the main impact on their business shortly, even more than Artificial Intelligence (68%), Big Data (54%) and Nanotechnology (44%) [4]. Estimates made in 2010 predicted that by 2020 the world would have approximately 50 billion IoT devices connected [5]. But more recent studies have revised this estimate forecast to 24.1 billion devices by 2030, with total revenue above US 1.5 trillion [6]. In this context, the cost per node unit is of paramount importance, and using the same substrate for the entire integration is simply indispensable. Still focusing on the mass production of devices, the use of low-cost substrates is essential. The lower cost of material and manufacturing, for instance, are pointed out as one of the main barriers to the growth of the use of IoT technology [7].

In the present paper, we put forward a step-by-step analytical procedure for designing bandpass filters exploring some design cheapening possibilities that could help to boost the IoT industry. In this sense, we propose using a substrate integrated waveguide (SIW) technology built with a low-cost and easily obtained material, the FR-4.

To illustrate our study, we chose a bandpass filter using SIW technology with an iris inductive window. The referred topology is well known and widely used, making it a suitable case for comparing the results obtained and those available in the current literature [8], [9]. The substrate used in these referred studies is the Rogers RT Duroid 5870® laminates, which are very efficient for microwave circuits, but whose price can reach a few dozen times higher than the FR-4. That significant cost difference in substrate material has motivated us to invest time in researching the utilization of low-cost laminates such as the FR-4 in microwave circuits. We also wanted to guide our research to add knowledge in a rapidly developing area that is the internet of things (IoT). So, we design our filter to operate at a frequency below 6 GHz [10].

Our goal will be to describe the design process for the microwave bandpass filter in SIW technology. In Fig. 1, we can see one general SIW body representation, a filter constituent part we want to design. Throughout the text, we will describe the theoretical modelling of each of the filter components: the 50-ohm line, the tapered impedance transition, the waveguide body, and calculate the Iris windows parameters.

Brazilian Microwave and Optoelectronics Society-SBMO *received 15 Apr 2021; for review 15 May 2021; accepted 2 Dec 2021*
Brazilian Society of Electromagnetism-SBMag *ISSN 2179-1074*

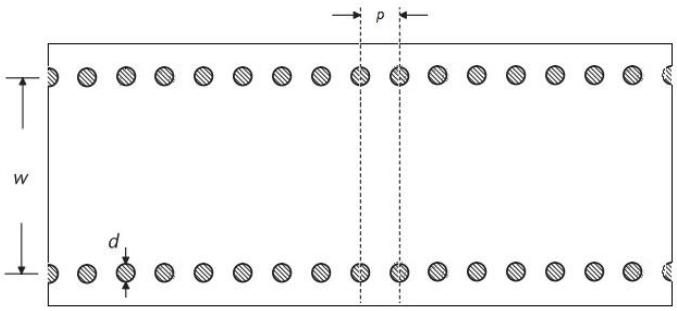

Fig. 1. SIW general structure with its main physical parameters

We organized the present paper as follows: In Section II, we review the basics of a SIW structure and its main parameters. Then, we briefly discuss dielectric materials and present the FR-4 main features. Section III is the present contribution core and brings the general steps and equations to reach the filter parameters. The SIW filter calculations are presented in detail. In Section IV, we discuss the computational simulations, prototype construction, and measurement results, analyzing the possible strategies to work around the problems we have found. In the last section, we added some remarks and final comments about our research as article conclusion.

II. FUNDAMENTALS OF SIW

A. Understanding the physical parameters

Fig. 2 illustrate the fundamental geometric parameters involved in the design of a SIW. The SIW structure features two rows of metalized holes, with a diameter d, spaced with a distance a_{eff}, where the orifices are spaced periodically by a distance p. The parameter h is the substrate thickness. The two metallic layer's function is to confine the electromagnetic wave inside the waveguide. It plays the same role as the sidewalls in a traditional rectangular metallic waveguide [3].

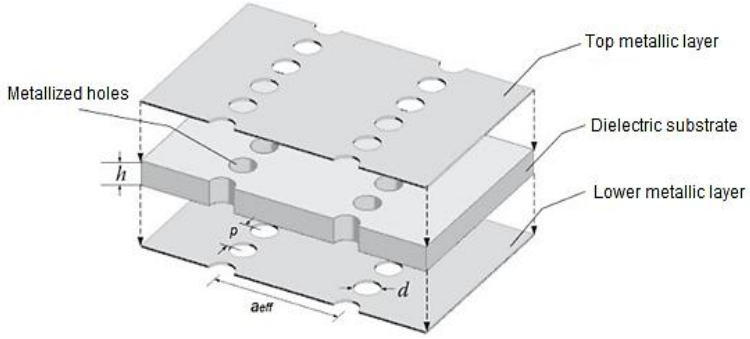

Fig. 2. Fraction of a waveguide that represents the SIW structure and main parameters. (Source: modified from [11])

B. Choosing the most suitable substrate

The material used as a substrate is an essential element in the microwave circuit design. The market offers a wide variety of options, but as explained in [12], the strategy of choosing the better-suited material takes into account mechanical, thermal, and electromagnetic features in addition to economic criteria. To ease the substrate choice, we can ask some questions aiming to guide the designer on the best alternative path:

Brazilian Microwave and Optoelectronics Society-SBMO *received 15 Apr 2021; for review 15 May 2021; accepted 2 Dec 2021*
Brazilian Society of Electromagnetism-SBMag *ISSN 2179-1074*

• Could the substrate cost under consideration justify the circuit or system cost?

• What frequency bands are involved? (It will strongly influence the dielectrics thickness and the ideal dielectric material permittivity).

• Metallic surface parameters are good enough to keep the conductor losses tolerable.

• Are the mechanical strength and thermal conductivity adequate for the application in question?

• Do the substrate has enough area to accommodate the electronics needed, considering mechanical limitations, complexity, and circuits diversity, in addition to the operating frequency limits?

Of course, the list above is for reference only. It is not exhaustive, nor it intends to be a checklist. Designers should formulate other questions or even neglect them, according to the complexity of each design.

C. The FR-4 substrate

The flame-retardant formulation number 4 class of materials, known by the acronym FR-4, is composed of fibreglass and an epoxy resin. It has high resistance to bending, heat, and humidity, commercially used in printed circuit boards and electronic equipment in general. It can have application in high-frequency circuits, and if the device has good loss tolerance is possible to use the FR-4 beyond 5 GHz. However, for these cases, losses will increase rapidly with rising frequency [13].

At microwave frequencies, the dielectric losses overcome the metallic conductor losses. Typical microstrip transmission lines exhibit a loss of 0.03 dB/cm/GHz for 1.6 mm thick substrate material. Because of dielectric loss dominance, the attenuation increases almost linearly with increasing frequency over a wide range. In such a case, the value is approximately 0.5 dB per wavelength [13]. In Fig. 3, we can see a chart with a comparison between the signal attenuation measured for a 200 mm long transmission line fabricated with the FR-4 (ε_r = 4.4 and $tan\ \delta$ = 0.02) and other two distinct dielectric materials (dielectric D1, with ε_r = 3.7 and $tan\ \delta$ = 0.002 and dielectric D2, with ε_r = 3.8 and $tan\ \delta$ = 0.005) [14]. Notice that the FR-4 material is much more dissipative than the other two materials under consideration, and the rate of dissipation is nearly constant over the frequency range shown.

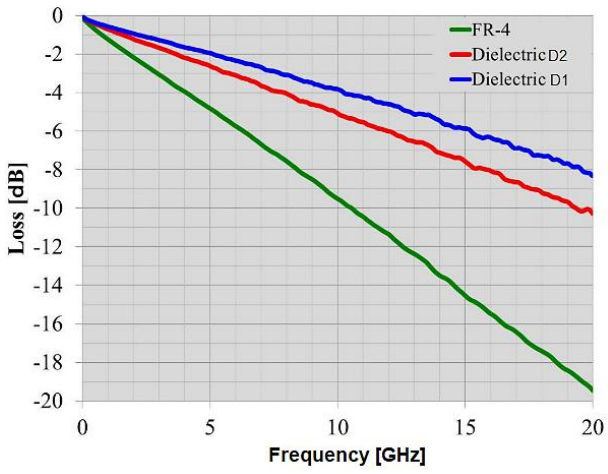

Fig. 3. Comparison of measured signal losses in distinct dielectric materials and the FR-4 (Source: [14])

ISSN 2179-1074

The FR-4, like other dielectric substrates commonly used in printed circuits, is a composite material. The precise composition of these materials can present variations, depending on the manufacturer and the production batch. In the case of FR-4, it has been found that different samples displayed values of relative dielectric constant ranging from 4.1 to 4.9 [13]. The author of Ref. [13] also points out that these distributions are not uniform. We can assume a ±5% variation in this parameter as a rule of thumb (as an example, a substrate with a dielectric constant of 4.2 may have a dielectric constant ranging between 4.2 ± 0.21).

For high-frequency transmission systems and signals with high bit rates (implying large bandwidths), the dielectric constant and the substrate thickness must be precisely known and must be regular and homogeneous in the parts used. Therefore, the FR-4 substrate is only suitable for a limited number of microwave applications [12]. Fig. 4 shows the FR-4 relative permittivity as a function of frequency for different glass reinforcements and resin percentage. Notice that the relative permittivity varies appreciably with increasing frequency.

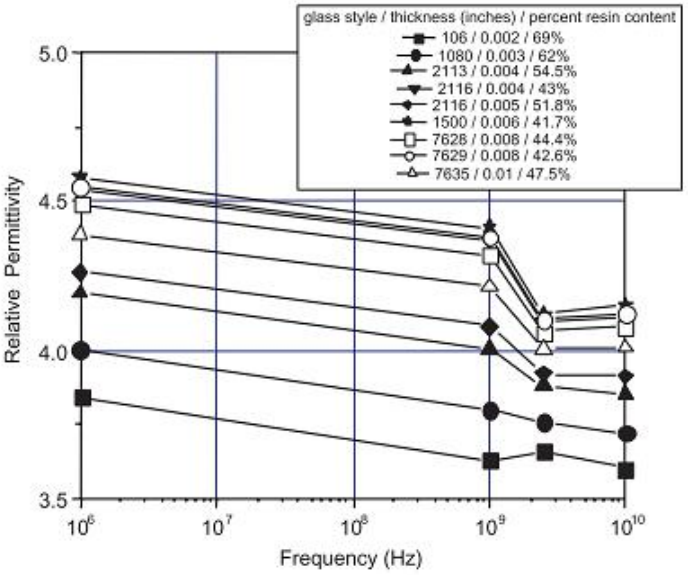

Fig. 4. Behavior of FR-4 relative permittivity in high frequencies with different glass and percentage of resin. (Source: [15])

In terms of cost, the FR-4 presents a huge difference concerning other substrates used in microwave circuits. The PCB price can vary according to several characteristics, such as the number of samples ordered, the substrate thickness, and due logistical and tax issues. However, despite its poor performance for microwave circuits, the FR-4 can be a few dozen times cheaper than other materials, and this cost disparity is enough motivation for research.

III. WAVEGUIDE AND FILTER DESIGN

A. Filter specification

As noted in the introduction, our goal was to design a filter compatible with IoT circuits. Such conditions lead us to specify our filter in the operating frequency range between 2.4 GHz and 6 GHz.

However, as we discuss before, high-frequency substrates are expensive. Thus, thinking to lower

received 15 Apr 2021; for review 15 May 2021; accepted 2 Dec 2021

ISSN 2179-1074

the cost of the project, we chose the FR-4 as a substrate. It is a material that, besides being low cost, is widely available.

We are aware that FR-4 imposes some limitations to high-frequency circuits due to dielectric losses, as discussed in Section II-C. Once we decided to use the FR-4 as a dielectric material, some concerns became important in our decisions: filters that are too large physically may be suitable neither due to the attenuation per unit length and the insertion losses that would be too large (see Fig. 3) nor with remarkably high central frequencies, because of the frequency dispersion (see Fig. 4).

Therefore, we chose 2.85 GHz as the central frequency, as it is within the standard specification we targeted, and it would not result in a filter as large physically, in addition to avoiding large dispersions at higher frequencies.

The filter bandwidth in our experiment is 100 MHz, resulting in a quality factor of 28.5. From the central frequency F_0 and the bandwidth, we obtain the frequencies F_1 and F_2, which are 2.8 GHz and 2.9 GHz (the cut-off frequencies, see Fig. 5).

We set the value of -45 dB for the attenuation in the rejection band. This value forces a low-order filter, resulting in a physically smaller circuit. We also fixed the return loss at order -10 dB and the insertion loss in the operating band of -2.5 dB. In Fig. 5, we can see the resulting mask with the reference curve for our filter.

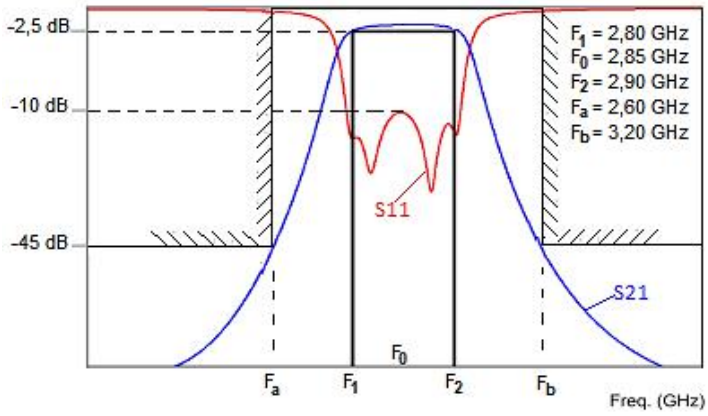

Fig. 5. Bandpass filter mask specification (Source: modified from [16])

B. The 50-ohm line

As discussed earlier, the SIW waveguide is based on microstrip technology. Therefore, the first filter design step consists of the 50-ohm microstrip line calculation. Fig. 6 shows the main physical parameters of a simple microstrip circuit that are significant for the project.

We found the method for calculating a microstrip line in [17]. The design input data are the characteristic impedance Z_0, the substrate thickness h, and the substrate relative dielectric constant ε_r. Using these parameters, we can calculate the microstrip line width w value, with the ratio w/h and using (1) or (2), as the case may be.

ISSN 2179-1074

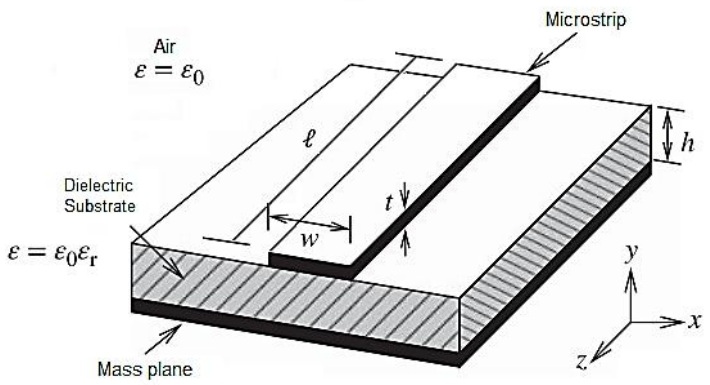

Fig. 6. Physical parameters of a microstrip line (Source: modified from [12])

For w / h < 2 :

$$\frac{w}{h} = \frac{8e^{(A)}}{e^{(2A)} - 2},$$

where:

$$\mathrm{A} = \frac{\mathrm{Z}_0}{60}\sqrt{\frac{\varepsilon_r + 1}{2}} + \frac{\varepsilon_r - 1}{\varepsilon_r + 1}\left(0.23 + \frac{0.11}{\varepsilon_r}\right), \tag{1}$$

For w / h > 2:

$$\frac{w}{h} = \frac{2}{\pi}\left[B - 1 - \ln(2B - 1)\right] + \frac{\varepsilon_r - 1}{2\varepsilon_r}\left\{\ln(B - 1) + 0.39 - \frac{0.61}{\varepsilon_r}\right\},$$

where:

$$B = \frac{377\pi}{2Z_0\sqrt{\varepsilon_r}}. \tag{2}$$

According to [17], the 50-ohm line length ℓ can be calculated for a phase shift of 270° by:

$$\ell = \frac{270°\left(\frac{\pi}{180°}\right)}{\beta}, \tag{3}$$

where β is the phase constant. For the ε_e computation, we will use the equations presented in [18]. In that study, the authors considered only the line geometry through the ratio *w*/h. The value of ε_e could still be refined by considering other parameters, like the microstrip metal thickness and the dispersion effects. However, in the present contribution, we will use the following expression:

$$\varepsilon_e = \frac{\varepsilon_r + 1}{2} + \frac{\varepsilon_r - 1}{2}\left(1 + 12\frac{h}{w}\right)^{-0.5}. \tag{4}$$

One parameter given for the calculation is the input impedance Z_0, which depends on the project context (being, therefore, an arbitrary value), which in our case, we chose to be 50 Ω. From de manufacturer datasheet, we still use the parameters dielectric constant ε_r and the dielectric thickness h. All mentioned parameters are relevant to determine the ratio *w*/*h* using equations (1) or (2).

C. The SIW body

Fig. 1 shows a SIW body schematic picture. The parameters d and p are the through-hole diameter, which will connect the waveguide to the ground plane, and the distance between the through-hole

received 15 Apr 2021; for review 15 May 2021; accepted 2 Dec 2021

ISSN 2179-1074

centres. In [12], the authors assert that the value of width d should be a small segment of the waveguide a_{eff}. We can assume, for the sake of simplicity, a widely used condition, i.e., $d < a_{eff} / 8$. However, in practice, the d value is limited by the availability of the tools to drill the through-holes [8]. The distance between the holes must respect the condition $p < 2d$ [12]. Greater p values may introduce significant signal attenuation due to failure in the electromagnetic wave confinement within the guide causing radiation losses. The waveguide effective width a_{eff} is calculated through the following equation:

$$a_{eff} = \frac{c}{2 f_{c10} \sqrt{\varepsilon_e}}, \tag{5}$$

where f_{10} is the waveguide cut-off frequency value in fundamental mode. It is possible to obtain f_{10} from the table of standards for rectangular waveguides in [15], according to the frequency range that the circuit desired will operate.

Fig. 7 shows a graph found in [20]. We can see a region in the d/λ_c and p/λ_c plane, where the SIW is equivalent to the rectangular waveguide, and it has a negligible radiation loss, besides, to not present flaws in the passband. We must design the waveguide body observing these rules described above to ensure it stays within the interest region showed in the graph.

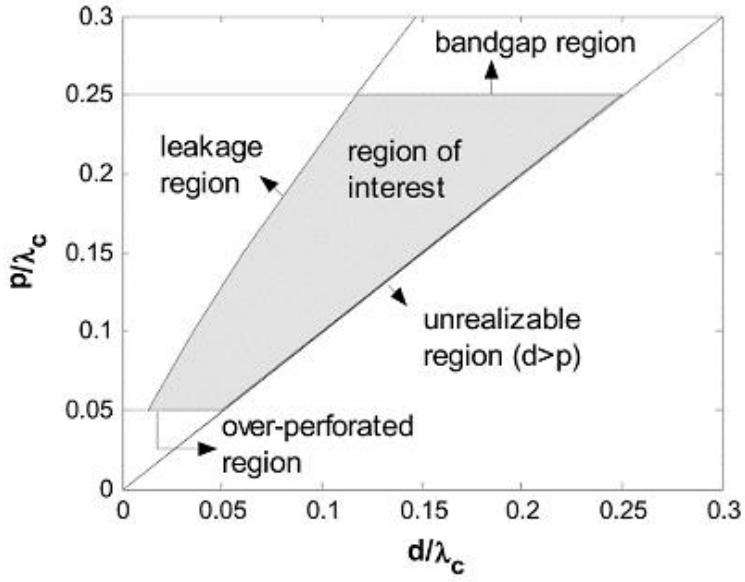

Fig. 7. Chart representing the geometric rules for waveguide body designing (Source: [20])

We calculated the guided wavelength value, using the following expression:

$$\lambda_c = \frac{2\pi}{\sqrt{\frac{\varepsilon_r (2\pi f)^2}{c^2} - \left(\frac{\pi}{a_{eff}}\right)^2}}, \tag{6}$$

the total (minimum) length value of the waveguide body is slightly larger than the wavelength λ_c value, always remembering that the waveguide must contain a few inductive windows that satisfy the filter specifications.

ISSN 2179-1074

To calculate the waveguide body, we need to define the metallic hole d diameter and the distance between holes p according to the design rules illustrated by the graph in Fig. 7. It is interesting to note that there are several possibilities for the values of p and d that work without impacting the filter response. Theoretically, once the conditions from the graph represented in Fig. 7 are guaranteed, the waveguide should work correctly.

To calculate the effective width a_{eff}, we use (5), where it is necessary to inform the cut-off frequency f_{10} value. Note that for the filter desired frequency range (with a frequency between 2.2 GHz to 3.3 GHz and a central frequency of 2.85 GHz), the cut-off frequency must be lower than 2.2 GHz. Consulting the table in [19], we found that our standard waveguide size is the WR340, which has a cut-off frequency in fundamental mode f_{10} = 1.736 GHz. The total waveguide width (dimension w_3, shown in Fig. 1), we may consider a_{eff} plus the space enough to accommodate the entire circuit, and for the line length calculation (dimension ℓ_3, shown in Fig. 1), we use (3).

As commented before, the waveguide body total length ℓ_3 depends on the distances between the inductive windows and is defined only after calculating these parameters. For now, we should only keep in mind that the waveguide body total length must be sufficient to accommodate all discontinuities in the chosen topology.

D. The tapered transitions

It is also necessary to integrate the SIW structures with the microstrip transmission line. The integration step is responsible for the impedance match between the 50-ohm line and the SIW waveguide body. The impedance transition width is a relevant point in the SIW filter design. Inaccuracy in this calculus might cause a considerable difference in the circuit performance.

There are several types of transitions described in [1] and [21]. In our project (since we are using microstrip at "low" microwave frequencies), we choose the conical transition integration.

In Fig. 8, we illustrate the schematic of a SIW, displaying the physical parameters to be calculated. Note the width w_1 matches the microstrip 50-ohm line width already calculated, and the width w_2 is the parameter we want to find. The length ℓ_2 calculation uses the equation (3). From [21], we found the following equations to calculate the transition width w_2:

$$\frac{1}{w_1} = \left\{ \begin{array}{c} \dfrac{60}{\eta h}\ln\left(8\dfrac{h}{w_2}+0.25\dfrac{w_2}{h}\right) \\ \dfrac{120\pi}{\eta h\left[\dfrac{w_2}{h}+1.393+0.667\ln\left(\dfrac{w_2}{h}+1.444\right)\right]} \end{array} \right\}, \tag{7}$$

$$\frac{1}{w_1} = \frac{4.38}{a_{eff}} e^{-0.627\frac{\varepsilon_r}{\frac{\varepsilon_r+1}{2}+\frac{\varepsilon_r-1}{2}\frac{1}{\sqrt{1+12\left(\frac{h}{w_2}\right)}}}}$$

ISSN 2179-1074

Where, $\eta = \sqrt{\mu_0/\varepsilon_0}$ the substrate relevant electromagnetic parameters (thickness h and relative dielectric constant, ε_r) and the microstrip 50-ohm width w_1 are known. Finally, we can then solve (7) and arrive at the width w_2 value. We found in [22] that solves the equations in a graphic form that quate simplifies the solution visualization. We reproduce the graph here in Fig. 9 with some modifications. We can find the value of w_2 in the intersection between curves.

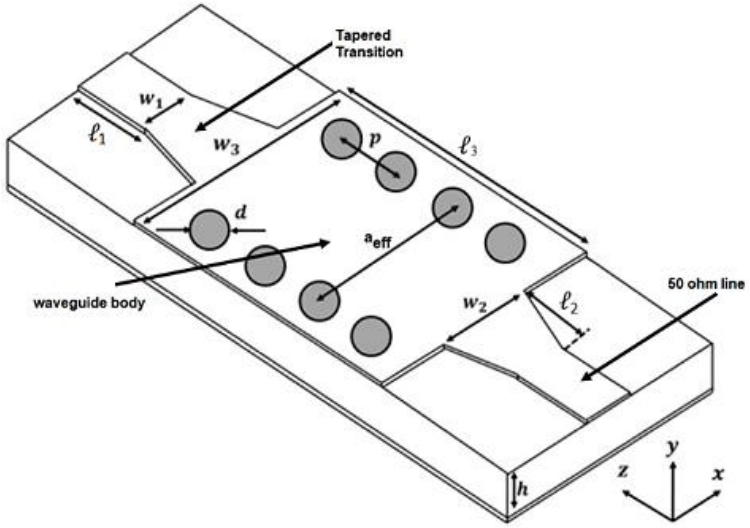

Fig. 8. Basic schematics with main physic parameters of a SIW (Source: modified from [8])

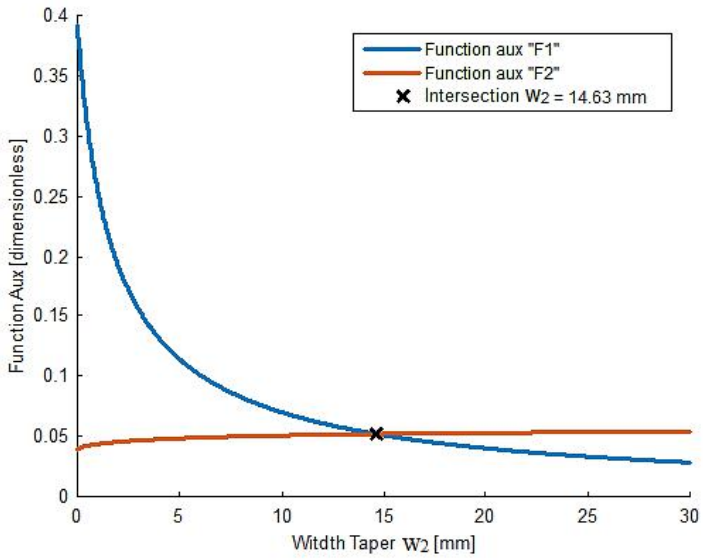

Fig. 9. We can find the tapered transition width w_2 in the curve's intercession.

E. Filter prototyping and the bandpass filter design

We can move on to the next step of the project: the filter design, which consists of calculating the low-pass prototype, scaling and converting the filter. We will utilize the frequency values seen in the mask of Fig. 5. The equations below describe the steps to calculate the filter prototype parameters. We use (08) and (09), to calculate the impedance inverters. We will use this data to calculate the resonant

ISSN 2179-1074

cavities physical parameters of our filter. Here, the parameter Z_0 (50 Ω) is the input impedance, and g_n are the elements normalized for the chosen Chebyshev 0.01 ripple response and can be found in [17]. The parameter w is the fractional bandwidth, calculated in (11). The generator impedance value is the standard w_1'=1. To calculate the average guided wavelength λ_{g0}, we use (10), and the wavelength values λ_{g1} and λ_{g2}, are calculated by (06). With (12), we calculate the fractional guided wavelength bandwidth and the normalized prototype frequencies w'/ w_1', as described by [23].

$$\frac{K_{n,n+1}}{Z_0} = \sqrt{\frac{\pi}{2}\frac{w_\lambda}{g_n g_{n+1} w_1^{'}}}, \tag{8}$$

$$\frac{K_{j,j+1}}{Z_0} = \frac{\pi w_\lambda}{2w^{'}}\frac{1}{\sqrt{g_j g_{j+1}}}, \tag{9}$$

$$\lambda_{g_0} = \frac{\lambda_{g_1} - \lambda_{g_2}}{2}, \tag{10}$$

$$w_\lambda = \frac{\lambda_{g_1} - \lambda_{g_2}}{\lambda_{g_0}}, \tag{11}$$

$$\frac{w^{'}}{w_1^{'}} = \frac{2}{w_\lambda}\left(\frac{\lambda_{g_1} - \lambda_{g_2}}{\lambda_{g_0}}\right). \tag{12}$$

Then, also from [23], we calculate the shunt reactances $X_{j,\,j+1}/ Z_0$, according to (13). Equation (14) and (15) directly calculate the length ℓ_1 of each resonant cavity.

$$\frac{X_{j,j+1}}{Z_0} = \frac{\dfrac{K_{j,j+1}}{Z_0}}{1-\left(\dfrac{K_{j,j+1}}{Z_0}\right)}, \tag{13}$$

$$\theta_j = \pi - \frac{1}{2}\left[\tan^{-1}\left(\frac{2X_{j-1,j}}{Z_0}\right) + \tan^{-1}\left(\frac{2X_{j,j+1}}{Z_0}\right)\right], \tag{14}$$

$$\ell_i = \frac{\theta_i \lambda_{g_0}}{2\pi}. \tag{15}$$

The diagram verification of the inductive window gap is also critical for the correct filter operation. The method to find the parameters was described by [24] and use the equation (13). In Fig. 10, we can see the chart plotted with the parameters for our bandpass filter. We observe the two points used to obtain the window opening parameters (0.45 and 0.27). We still need to multiply these values by a_{eff}, calculated by (5), and finally, we have the iris windows width.

There are still the distances between the inductive window to calculate. For the mentioned step, we use (14) and (15).

Brazilian Microwave and Optoelectronics Society-SBMO *received 15 Apr 2021; for review 15 May 2021; accepted 2 Dec 2021*
Brazilian Society of Electromagnetism-SBMag *ISSN 2179-1074*

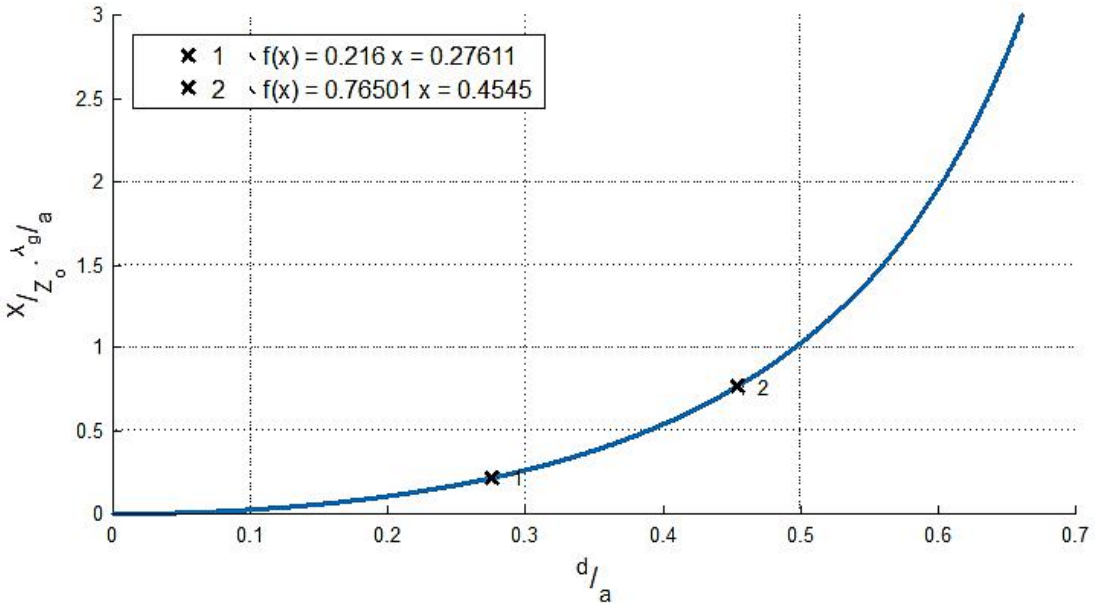

Fig. 10. Chart that uses the equations found in [24] and simplify the determination of Iris width.

In Fig.11, we present the final bandpass filter layout with all its constructive parameters, with values described in Table I.

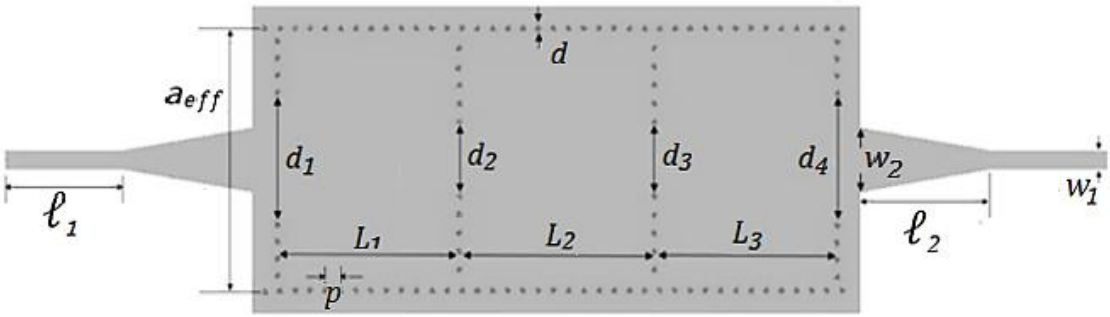

Fig. 11. Schematic showing all geometric parameters of the bandpass filter in SIW technology.

TABLE I. SIW FILTER PHYSICAL PARAMETERS

Parameters	Value	Unit
Dielectric thickness (h)	1.6	mm
Dielectric Rel. permittivity. (ε_r)	4.5	
Dielectric Tangential loss (δ)	0.027	
Characteristic impedance (Z_0)	50	ohms
Width line 50 ohms (w_1)	2.94	mm
Length line 50 ohms (ℓ_1)	20.37	mm
Cooper thickness (t)	17.1	um
Length tapered transition (ℓ_2)	20.37	mm
Width transition (w_2)	14.62	mm
Width waveguide (a_{eff})	41	mm
Length waveguide (ℓ_3)	90	mm
Through-hole diameter (d)	1	mm
Through-hole length (p)	2.5	mm
Width IRIS window ($d1$=$d4$)	18.44	mm
Width IRIS window (d_2=d_3)	11.26	mm
Length IRIS Window (L_1=L_3)	25.88	mm
Length IRIS Window (L_2)	28.42	mm

ISSN 2179-1074

IV. PROTOTYPE SIMULATIONS AND MEASUREMENT

A. Material and methods

The computational tool we have chosen for the electromagnetic simulation is the ADS Momentum 3D Planar EM simulator from Keysight Technologies. ADS Momentum 3D is an electromagnetic simulator used for modelling and analyzing passive circuits. We use the manufacturer electrical parameters for the dielectric substrate simulation and, for the charts, uses the S parameters. To perform prototype measurements, we use a network analyzer from Keysight (ENA E5063A®). To implement connections, we use 50 ohms coaxial cables and SMA connectors. All those components were de-embedded using the Keysight toolkit. In Fig. 12, we can see the upper and lower prototype sides photo.

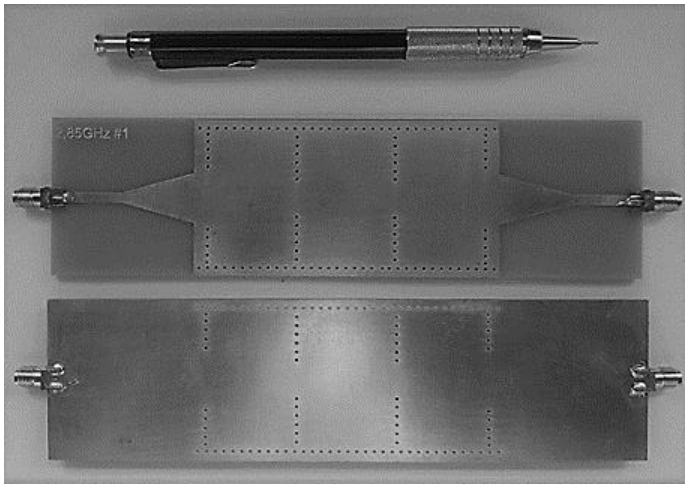

Fig. 12. Photo showing the prototype upper and lower sides.

B. Comparison between measurement and simulation

Analysing prototype measurement, we could consider the analytical method precision and how accurate the computational simulation would be concerning what was calculated.

Fig. 13 shows the prototype measurement compared with the reference curve (which has the design parameters specified initially) and the graphs obtained through electromagnetic simulation.

The simulation values were gathered directly from analytical equations, and we can see that it does not reach the specification. The picture clearly shows such behaviour, as we can see the discrepancies in the frequency shift and attenuation. The probable reason for the difference regarding the simulated curve frequency shift is the dispersion that the FR-4 material presents, which is quite significant, as we have seen, quite significant. We may observe that there is also a frequency shift between the simulated curve and the measurement. The phenomenon suggests a distortion between the dielectric constant parameter provided by the manufacturer (and which we use in our calculations) and the material dielectric constant. According to [13], it is common to have variations in the order of ±5% in the parameter value for FR-4 material, not only for materials from different manufacturers but even materials within the same batch, as commented earlier.

received 15 Apr 2021; for review 15 May 2021; accepted 2 Dec 2021

ISSN 2179-1074

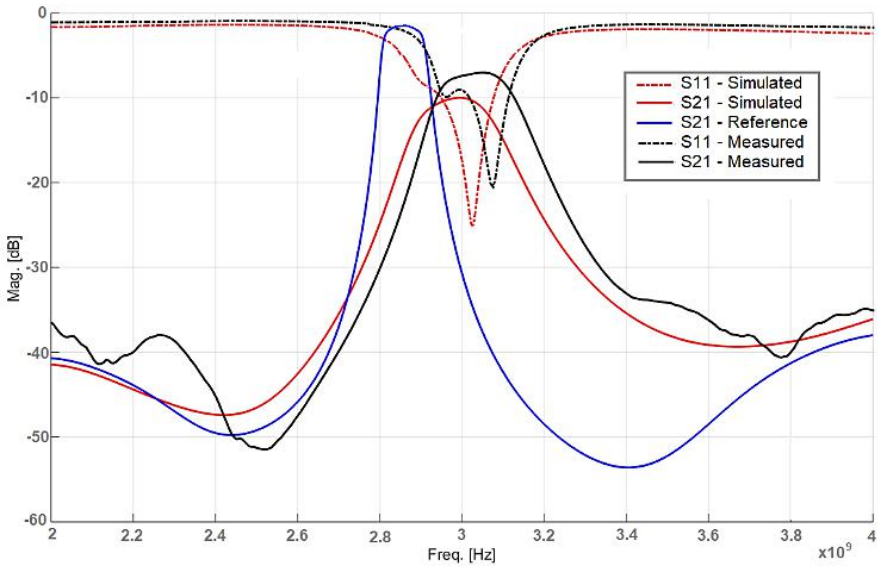

Fig. 13. Comparison between the prototype measuring, simulation, and reference curves.

We can also notice that the passband value, both for the simulated curve and the measurement, had a result quite out of target. Originally the passband was specified at 100 MHz, but the measured values for the simulated curve were 187 MHz and for the measured, 192 MHz.

Another relevant factor to observe concerns the attenuation in the passband in both curves: simulation and measurement. By the way, notice that the simulation presents a considerable attenuation concerning the measure. The reason for the attenuation may be the FR-4 dissipation factor (tangential loss), which according to the dielectric´s datasheet, is 0.027. Such value is remarkably high for the filter frequency range in question. The difference between the simulated curve and the measured curve suggests that the dissipation factor value provided in the FR-4 specification is not the same as the actual value that the material presents.

Although the results in Fig.13 show some deviation from the original specification and even considering the material used, the curves presented appear to be reasonable, as they are like other publications results, as in [9], [16] and [25].

C. Analysis

As suggested above, we raised the hypothesis that the differences in frequency in Fig. 13 could be caused by a discrepancy between the real material dielectric constant value and the value provided by the FR-4 manufacturer. According to [13], the relative permittivity value can vary from 4.1 to 4.9. With this information in mind, and to confirm whether our suspicions were well-founded, we plotted in Fig. 14 the simulation of our prototype for some values of dielectric constant in the indicated range.

Analyzing the curves, we found that the dielectric constant, ranging from 4.1 to 4.9, causes a frequency shift. We also see that the relative dielectric constant ε_r = 4.3 graph practically coincides with the measurement curve, which is an indication that the new data is the material's real relative dielectric constant value, instead of that provided by the manufacturer of ε_r = 4.5.

ISSN 2179-1074

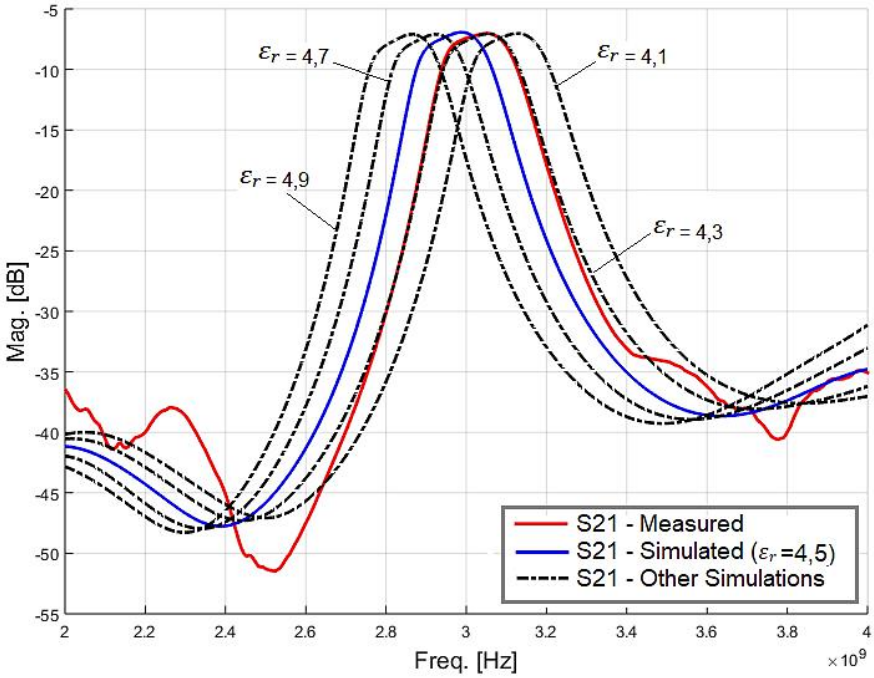

Fig. 14. Measured curve and simulations for different dielectric constants.

Following the same reasoning, we also did a simulation for the other parameter that showed a discrepancy between the simulation and the measurement: the dissipation factor. According to the work of [12], the parameter value can vary from 0.01 to 0.027 for the FR-4. Analysing the curves plotted in Fig. 15, we can see that the attenuation changes accordingly with the dissipation factor variation.

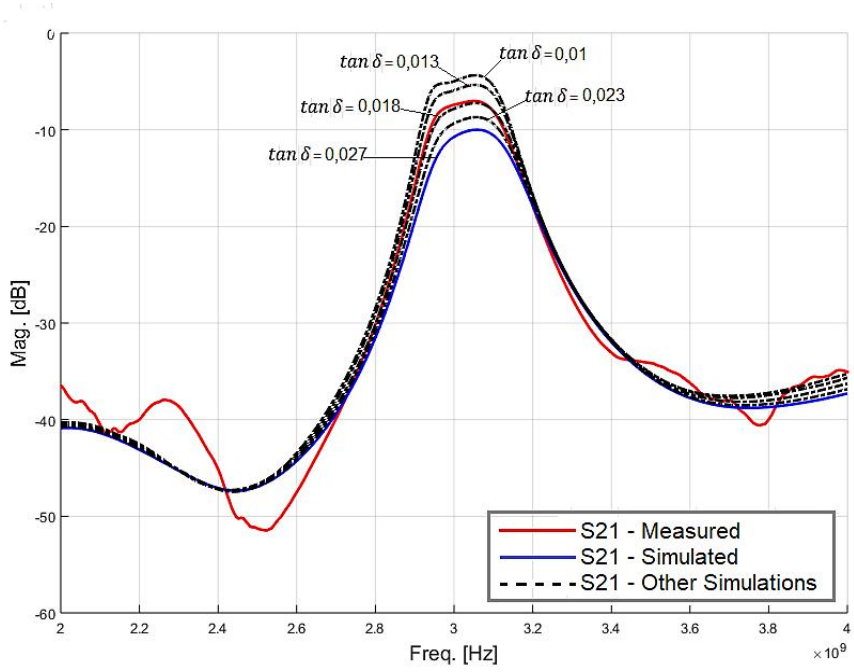

Fig. 15. Measured curve and Simulation curves for different dissipation factors.

We observe that the curve with the simulation for the dissipation factor of 0.018 almost coincides with the measurement value. The previously mentioned behaviour confirms our assumption that the

ISSN 2179-1074

dissipation factor value provided by the FR-4 manufacturer does not match with the actual material used. For the simulation, we have already used the correct relative dielectric constant value, 4.3.

The analysis of Fig. 14 and Fig. 15 leads us to the probable real values for the parameters of dielectric constant (ε_r = 4.3) and dissipation factor ($tan\ \delta$ = 0.018). We can now realize a new SIW prototype simulation with the improved parameters and compare it with the measured curve, shown in Fig. 13. Fig. 16 presents the new simulation for S21 (insertion loss) and S11 (return loss). We can see now that the curves are remarkably close to the measured curves for both: frequency and attenuation.

The analytical method presented in the article was developed originally for filters designed in rectangular metallic waveguide technology. There is vast literature studying the analytical equivalences between SIW technology and rectangular waveguides. We cite here the work of [26]. Regarding the accuracy of this equivalence, [21] reminds us that these analytical models are not perfect because capacitive effects in the SIW transitions are not considered. Indeed, for our experiment with FR-4, we had a good comprehension of these calculation inaccuracies and how they can cause distortions. However, we can conclude that with a full-wave electromagnetic simulation tool and precise dielectric parameters knowledge, it is possible to build prototypes of filters in SIW technology with reliability.

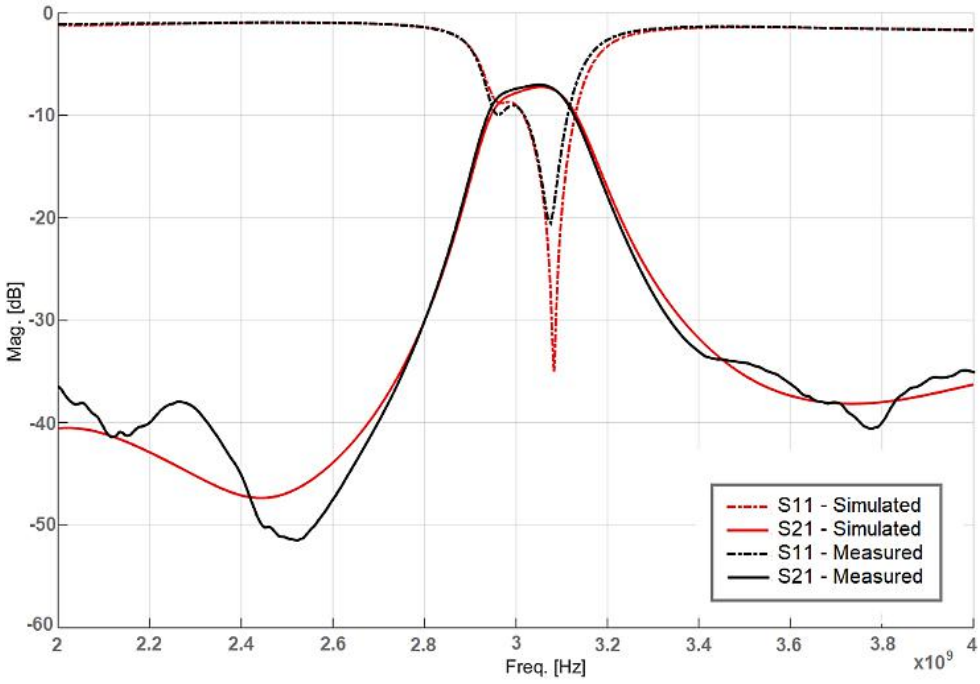

Fig. 16. After adjustments, the simulation and measurement curves look remarkably similar.

With the new electric parameters for the dielectric, we can recalculate the filter´s constructive parameters. To change them, we used the method described in the works of [8] and [27], which consists of manually adjusting these parameters directly in the filter layout in the simulation stage. The new physical measures already improved for the new prototype can be seen in Table II.

ISSN 2179-1074

TABLE II. SIW FILTER WITH NEW PHYSICAL PARAMETERS

Parameters	**Value**	**Unit**
Dielectric thickness (h)	1.6	mm
Dielectric Rel. permittivity. (ε_r)	4.3	
Dielectric Tangential loss (δ)	0.018	
Characteristic impedance (Z_0)	50	ohms
Width line 50 ohms (w_1)	2.94	mm
Length line 50 ohms (ℓ_1)	20.37	mm
Cooper thickness (t)	17.1	um
Length tapered transition (ℓ_2)	20.37	mm
Width transition (w_2)	14.62	mm
Width waveguide (a_{eff})	41	mm
Length waveguide (ℓ_3)	95	mm
Through-hole diameter (d)	1	mm
Through-hole length (p)	2.5	mm
Width IRIS window ($d1$=$d4$)	19.2	mm
Width IRIS window ($d2$=$d3$)	10.8	mm
Length IRIS Window (L1=L3)	29.6	mm
Length IRIS Window (L2)	30.7	mm

Fig. 17 illustrate a comparison between the simulation curve for the improved prototype with the reference curve. Examining the picture, we can observe that with the new parameters for the iris window and the adjusted resonant cavity length, we finally managed to get close to the reference values concerning the frequencies involved. The bandwidth result is also better (140MHz), and the filter quality factor is 20.3. Finally, the observed insertion loss amounts to -7 dB, and any improvements are limited by the used material dissipation factor. The new value we found (0.018) is still too high to approach the original specification.

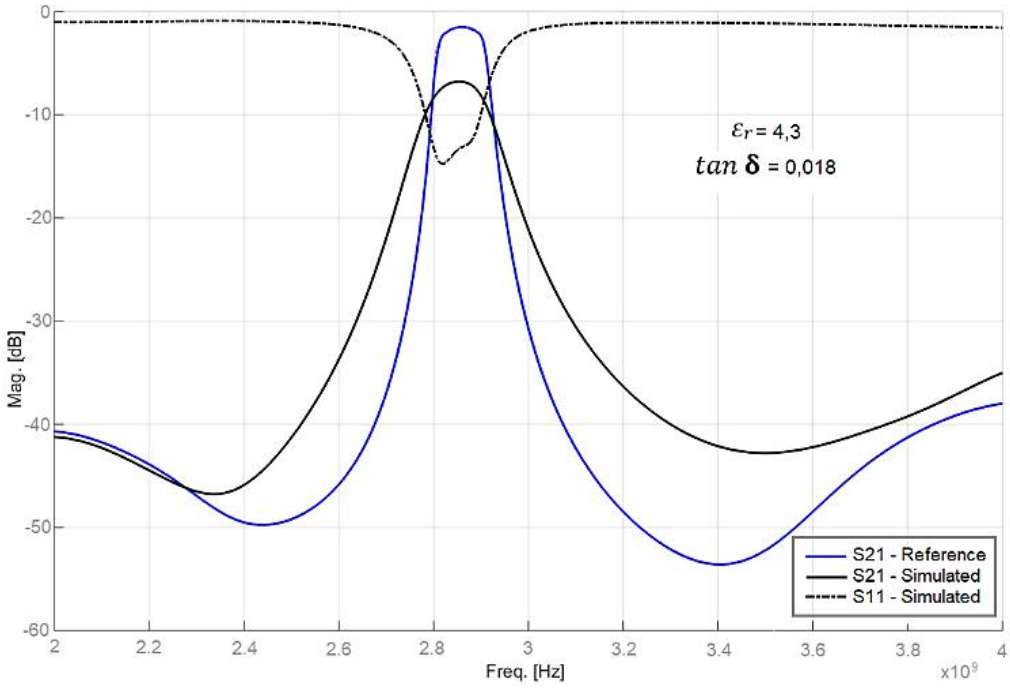

Fig. 17. Simulation curve (already with adjustments) compared with the initial specification curve.

The utilization of a less dissipative substrate would present better values for the bandwidth and the filter quality factor and make it more selective. This behaviour can be found in other published works, as in [9] and [28].

ISSN 2179-1074

V. CONCLUSION

In the present paper, we show a step-by-step process for designing a microwave bandpass filter in SIW technology, using a low-cost substrate. Throughout the text, we have introduced the theoretical modelling for each filter component, performed the computational simulations using full-wave software, and realized the measurements on the built prototype. We noticed the discrepancies between the theoretical result and the measurements executed, made the necessary adjustments, and reached satisfactory results. The low-cost substrate we chose, the FR-4, is very close to the design expectations, although it is sure that less dissipative substrates would perform better. However, for low-cost applications, the use of FR-4 material is widely justified.

REFERENCES

[1] F. Parment, "High performance multilayer Substrate Integrated Waveguide (SIW) technics for low-cost millimeter-wave circuits," Université Grenoble Alpes, 2017.

[2] J. Hirokawa and M. Ando, "Single-layer feed waveguide consisting of posts for plane TEM wave excitation in parallel plates," *IEEE Transactions on Antennas and Propagation*, vol. 46, no. 5, pp. 625–630, 1998.

[3] H. Uchimura, T. Takenoshita, and M. Fujii, "Development of a 'laminated waveguide,'" *IEEE Trans. Microw. Theory Tech.*, vol. 46, no. 12, pp. 2438–2443, 1998, DOI: 10.1109/22.739232.

[4] M. J. Haber and B. Hibbert, "Internet of Things (IoT)," *Privil. Attack Vectors*, pp. 139–142, 2018, DOI: 10.1007/978-1-4842-3048-0_14.

[5] Ericsson, "CEO to shareholders: 50 billion connections 2020," *https://www.ericsson.com/en/press-releases/2010/4/ceo-to-shareholders-50-billion-connections-2020*, 2010. https://www.ericsson.com/en/press-releases/2010/4/ceo-to-shareholders-50-billion-connections-2020.

[6] M. Hatton, "The IoT in 2030: 24 billion connected things generating $1.5 trillion Title," *IoT.Business.News*, 2020. https://iotbusinessnews.com/2020/05/20/03177-the-iot-in-2030-24-billion-connected-things-generating-1-5-trillion/.

[7] A. Behrendt, E. De Boer, T. Kasah, B. Koerber, N. Mohr, and G. Richter, "Leveraging Industrial IoT and advanced technologies for digital transformation," *McKinsey Co.*, pp. 1–75, 2021.

[8] R. C. Caleffo, "Estudo e aplicação de guias de ondas integrados ao substrato em frequencia de microondas," Universidade de São Paulo, São Paulo, 2016.

[9] E. Troy, "Why FR-4 Is Often Inadequate for RF Design," *Copyright 2014 Aerospace Consulting LLC*, 2014. https://rfandmicrowavedesign.com/fr-4-often-inadequate.html (accessed Feb. 19, 2021).

[10] S. Cirani, G. Ferrari, M. Picone, and L. Veltri, "Standards," in *Internet of Things*, John Wiley & Sons Ltd, Ed. Chichester, UK: John Wiley & Sons, Ltd, 2018, pp. 9–77.

[11] Y. J. Cheng, *Substrate Integrated Antennas and Arrays*. CRC Press, 2018.

[12] T. C. Edwards and M. B. Steer, *Foundations for Microstrip Circuit Design*. Chichester, UK: John Wiley & Sons, Ltd, 2016.

[13] T. H. Lee, *Planar Microwave Engineering*, Cambridge. Cambridge: Cambridge University Press, 2004.

[14] E. Liew, T. Okubo, T. Sudo, T. Hosoi, H. Tsuyoshi, and F. Kuwako, "Signal transmission loss due to copper surface roughness in high-frequency region," in *IPC APEX EXPO 2014: New Ideas... For New Horizons*, 2014, no. 4, [Online]. Available: http://www.scopus.com/inward/record.url?scp=84919935727&partnerID=8YFLogxK.

[15] IPC-2141A, "Design Guide for High-Speed Controlled Impedance Circuit Boards," *Ipc*, no. April 1996, pp. 16–19, 2004.

[16] J. Garreau *et al.*, "Ultra-compact X-band SIW filter in LTCC technology using high permittivity substrate for a space application," in *2012 IEEE/MTT-S International Microwave Symposium Digest*, Jun. 2012, pp. 1–3, DOI: 10.1109/MWSYM.2012.6258416.

[17] D. M. Pozar, *Microwave Engineering, 4th Edition*, 4th ed. Danvers, MA, 2012.

[18] J.-S. Hong, *Microstrip Filters for RF/Microwave Applications*, vol. 66. Hoboken, NJ, USA: John Wiley & Sons, Inc., 2011.

[19] EverythingRF, "everythingRF," *Copyright 2020 © everything RF All Rights Reserved*, 2020. https://www.everythingrf.com/tech-resources/waveguides-sizes (accessed Mar. 27, 2021).

[20] D. Deslandes and Ke Wu, "Accurate modelling, wave mechanisms, and design considerations of a substrate integrated waveguide," *IEEE Trans. Microw. Theory Tech.*, vol. 54, no. 6, pp. 2516–2526, Jun. 2006, DOI: 10.1109/TMTT.2006.875807.

[21] D. Deslandes, "Design equations for tapered microstrip-to-Substrate Integrated Waveguide transitions," in *2010 IEEE MTT-S International Microwave Symposium*, pp. 704–707, May 2010. DOI: 10.1109/MWSYM.2010.5517884.

[22] X. C. Megias, "Permittivity measurement of biological samples using SIW devices," Universitat Politecnica de Catalunya, 2017.

[23] G. L. Matthaei, L. Young, and E. M. Jones, *Microwave filters, impedance-matching networks, and coupling structures*, Artech Hou. Norwood, MA: McGraw-Hill Book Company, INC., 1980.

Brazilian Microwave and Optoelectronics Society-SBMO *received 15 Apr 2021; for review 15 May 2021; accepted 2 Dec 2021*
Brazilian Society of Electromagnetism-SBMag *ISSN 2179-1074*

[24] N. Marcuvitz, *Waveguide Handbook*. The Institution of Engineering and Technology, Michael Faraday House, Six Hills Way, Stevenage SG1 2AY, UK: IET, 1986.

[25] A. Glise *et al.*, "LDS Realization of High-Q SIW Millimeter Wave Filters with Cyclo-Olefin Polymers," *Appl. Sci.*, vol. 8, no. 11, p. 2230, Nov. 2018, DOI: 10.3390/app8112230.

[26] D. Wang, Y. L. Chow, K. Deng, and W. Che, "Analytical equivalence between a substrate-integrated waveguide and rectangular waveguide," *IET Microwaves, Antennas Propag.*, vol. 2, no. 1, pp. 35–41, Feb. 2008, DOI: 10.1049/iet-map:20060283.

[27] F. Parment, A. Ghiotto, T.-P. Vuong, J.-M. Duchamp, and K. Wu, "Low-loss air-filled Substrate Integrated Waveguide (SIW) band-pass filter with inductive posts," in *2015 European Microwave Conference (EuMC)*, Sep. 2015, pp. 761–764, DOI: 10.1109/EuMC.2015.7345875.

[28] N. H. Nguyen, F. Parment, A. Ghiotto, K. Wu, and T. P. Vuong, "A fifth-order air-filled SIW filter for future 5G applications," in *2017 IEEE MTT-S International Microwave Workshop Series on Advanced Materials and Processes for RF and THz Applications (IMWS-AMP)*, Sep. 2017, vol. 2018-Janua, no. September, pp. 1–3, DOI: 10.1109/IMWS-AMP.2017.8247355.

received 15 Apr 2021; for review 15 May 2021; accepted 2 Dec 2021

ISSN 2179-1074